Evaluation of Low-Dose CT Perfusion for the Liver using Reconstruction of Difference

Saeed Seyyedi, Eleni Liapi, Tobias Lasser, Robert Ivkov, Rajeev Hatwar, J. Webster Stayman

Abstract— CT perfusion imaging of the liver enables the evaluation of perfusion metrics that can reveal hepatic diseases and that can be used to assess treatment responses. However, x-ray radiation dose limits more widespread adoption of liver CT perfusion studies as a diagnostic tool. In this work we assess a model-based reconstruction method called Reconstruction of Difference (RoD) for use in low-dose CT perfusion of the liver. The RoD approach integrates a baseline non-contrast-enhanced scan into the reconstruction objective to improve image volumes formed from low-exposure data. Simulation studies were conducted using a digital human liver phantom based on segmented anthropomorphic CT images and time-attenuation curves derived from CT perfusion studies in a rabbit model. We compare the RoD method with standard FBP and penalized-likelihood reconstructions through an evaluation of individual image volumes in the low-dose enhanced liver volume sequence as well as in an evaluation of perfusion maps. Specific perfusion metrics include hepatic arterial perfusion (HAP), hepatic portal perfusion (HPP) and perfusion index (PI) parameters computed using the dual-input maximum slope method (SM). The quantitative and qualitative comparisons of reconstructed images and perfusion maps shows that the RoD approach can significantly reduce noise in low-dose acquisitions while maintaining accurate hepatic perfusion maps as compared with traditional reconstruction methods.

Index Terms—Low-Dose CT, Prior-image-based Reconstruction, Sequential Imaging.

I. INTRODUCTION

CT perfusion (CTP) is a functional imaging modality based on sequential scanning of the same tissue before, during, and after the administration of a contrast agent to trace temporal changes in tissues of interest. Recent advancements in CT imaging including larger detectors and wide cone angles, have enabled CTP for stroke imaging of the brain, cardiac events and liver abnormalities [1]. Liver CTP permits evaluations of liver function, damage, and disease including diagnoses related to hepatocellular carcinoma and the assessment of surgical interventions [2], [3]. Recent work suggests that liver CTP is a potential biomarker for assessing tumor response to specific therapies [4]. More widespread adoption of liver CTP in clinical trials to assess its potential as a biomarker as well as broader clinical use have been hampered by concerns over radiation exposure.

A variety of strategies have been proposed to limit radiation exposure including the individualization of scanning parameters (e.g. based on patient size), modification of tube current or voltage throughout the observation period [5], [6]. However, decreasing the x-ray radiation dose reduces CT image quality with increased noise and possible streak artifacts which lowers the clinical and diagnosis utility of the scan. Model-based iterative reconstruction (MBIR) techniques have been proposed as one potential solution to reduce image noise and artifacts under reduced of tube current conditions, permitting lower effective dose values [7]. In Negi et al. [8], the Adaptive Iterative Dose Reduction (AIDR) reconstruction approach was found to reduce image noise and while preserving hepatic perfusion parameters values as compared with higher exposure filtered-backprojection (FBP) images.

Prior-image-based reconstruction (PIBR) approaches have been studied by a number of groups and have shown the potential for dose reductions even greater than traditional MBIR methods. These approaches incorporate patient-specific anatomical information from previously acquired scans of the same patient directly into a reconstruction objective function whose solution is approximated iteratively. Example PIBR methods include prior-image-constrained compressed sensing (PICCS) [9] and prior-image-registered penalized-likelihood estimation (PIRPLE). [10] Both of these techniques use a high quality prior image volume to help reconstruct low exposure or under-sampled projection data. PICCS has previously been investigated for small animal CTP [11]. A modification of PIRPLE with deformable registration has been used to reduce x-ray exposures in lung nodule surveillance by more than an order of magnitude [12]. Recently, Pourmorteza et al. [13] proposed a novel Reconstruction of Difference (RoD) technique that uses a penalized likelihood objective to directly reconstruct the difference between a prior image and the current anatomy enabling direct reconstructions of anatomical change (analogous to digital subtraction angiography) with reduced noise.

In this work, we apply the RoD method to low-dose CTP data. The approach is investigated in simulation studies using an anthropomorphic phantom with realistic time attenuation curves (TACs) for different tissue types. We analyze imaging performance in individual reconstructions in the imaging sequence from contrast injection, through uptake, and washout, and perform a perfusion analysis to compare several perfusion metrics including hepatic arterial perfusion (HAP), hepatic portal perfusion (HPP) and perfusion index (PI). The RoD approach is compared with traditional FBP and penalized-likelihood (MBIR) reconstructions.

S. Seyyedi is with Computer Aided Medical Procedures and Chair of Biomedical Physics, Technical University of Munich, Munich, 85748 Germany.
E. Liapi is with the Department of Radiology and Radiological Sciences, Johns Hopkins Hospital, Baltimore, MD 21205 USA.
T. Lasser is with Computer Aided Medical Procedures, Technical University of Munich, Munich, 85748 Germany.
R. Ivkov is with the Department of Radiation Oncology, Johns Hopkins Hospital, Baltimore, MD 21205 USA.
R. Hwatar is with the Department of Mechanical Engineering, Johns Hopkins University, Baltimore, MD 21205 USA.
J. W. Stayman is with the Department of Biomedical Engineering, Johns Hopkins University, Baltimore, MD 21205 USA (e-mail: web.stayman@jhu.edu).
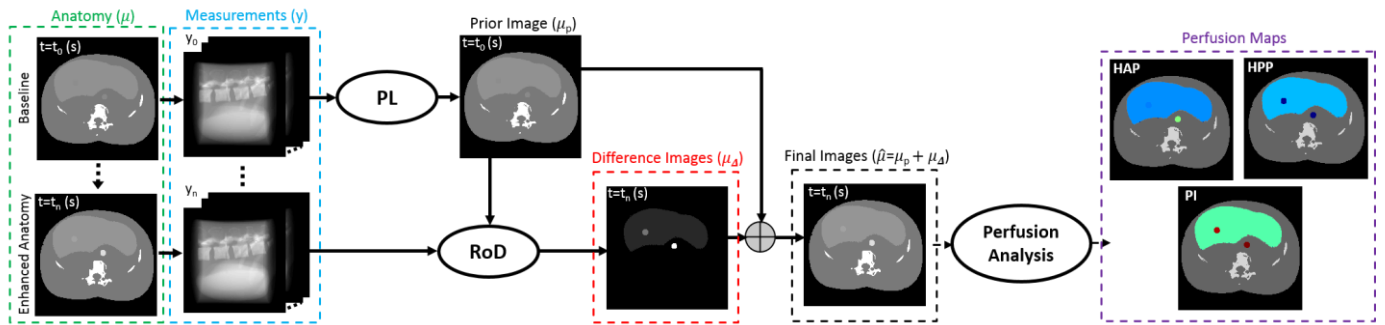
Figure 1: Overview of the acquisition and processing chain for CT perfusion using RoD. Differences images for each time point in the series are reconstructed relative to a high-quality non-contrast-enhanced baseline image. Estimates of the current anatomy may be formed by adding back the prior image, and subsequent perfusion analysis is applied to generate standard perfusion maps using different metrics.

II. METHODS

An illustration of the proposed acquisition and processing chain for liver CTP is shown in Figure 1. Tomographic measurements (y_n) are acquired over a range of time points $n = 0$ to N. These measurements cover a changing anatomy (μ_n) from an unenhanced volume (pre-iodine-injection) at $n = 0$, through uptake and washout of the contrast. A high-quality unenhanced baseline image (μ_0) serves as a prior image (μ_p) for input into RoD to reconstruct difference image volumes (μ_Δ) for all subsequent low-dose sequential data. These difference images can be used to form estimates of the current image anatomy ($\hat{\mu} = \mu_p + \hat{\mu}_\Delta$) at each time point. Subsequent perfusion analysis using standard computations on the entire image sequence is then used to create perfusion maps using various metrics.

A. Data Generation and Phantom Design

To evaluate the proposed acquisition and processing chain in simulation, a 4D phantom is required that has both realistic anatomical features and contrast dynamics. Specifically, to assess the ability to estimate temporal dynamics, it is necessary to generate data with time-attenuation curves (TACs) defining enhancement in liver.

Toward this end, we obtained TACs from a rabbit abdominal study that estimated smooth TACs for several different tissue types. Adult male New Zealand White rabbits (3.5 kg) were used in this study. Each animal received VX2 tumor implantation in the left lobe of the liver, and tumors were allowed to grow for 13-15 days prior to imaging. For CT perfusion, se-

dated rabbits were scanned using a 320-slice CT scanner (Aquilion One, Toshiba, Japan). Iodixanol (1.5 ml/kg, 320 mg I/ml Visipaque, GE Healthcare, Princeton, NJ) was injected at a rate of 1 ml/sec followed by a 7 ml saline flush at 1 ml/sec. The scan technique was 120 kVp, 80 mA and used 0.5 mm slices. The imaging sequence started after a 6 sec delay and was composed of scans at 2-sec intervals for the first 25 sec, and every 3 sec for an additional 42 seconds. Reconstructions were performed with Adaptive Iterative Dose Reduction 3D followed by registration (Body Registration, Toshiba Medical Systems, Tochigi, Japan) to account for motion during the scan.
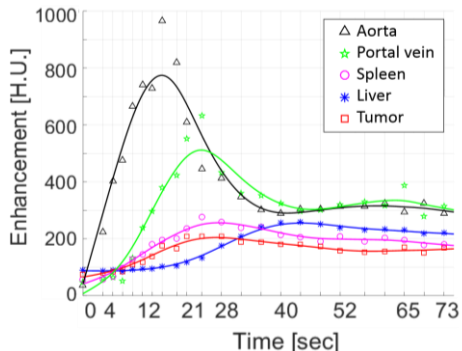
Rabbit TAC curves (Figure 2) were formed via manual identification of regions-of-interests – aorta, portal vein, spleen, healthy liver, and a liver tumor – followed by smoothing of the temporal series. These TACs were mapped onto an anthropomorphic phantom shown in Figure 3. This phantom covers an axial extent of 20.48 cm and includes a simulated spherical tumor of 12 mm diameter. Temporal sampling for data generation followed a similar protocol as that used in the animal model with denser sampling at the beginning of the sequence. The exact sampling pattern is shown in Figure 4 starting with an initial non-enhanced scan followed by a 4 sec delay and 7 scans over 12 sec, a 6 sec delay followed by 8 scans over 28 sec, a 5 sec delay, and finally 5 scans over 16 sec.

B. Hepatic Perfusion Analysis

We use the dual-input maximum slope method [14] to calculate the perfusion metrics for both the baseline truth as well as processed data. The slope method is commonly used in the eval-

Figure 2: TACs obtained from an abdominal scan of a rabbit animal model with HCC are obtained using a smooth fit to attenuation values at individual time points. A region of interest in five tissue types allowed estimation of TACs for the aorta, portal vein, spleen, healthy liver tissue, and a liver tumor.
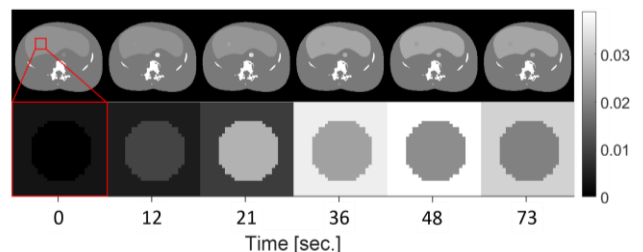
Figure 3: 4D Digital liver phantom designed for CT perfusion studies. Single slices and a zoomed region around a simulated tumor are shown for six time points in the sequence.
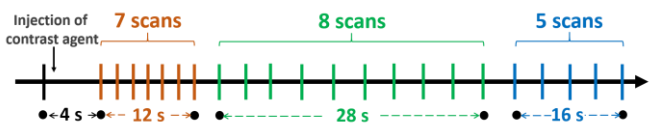
Figure 4: Temporal sampling in the CT perfusion simulation study.
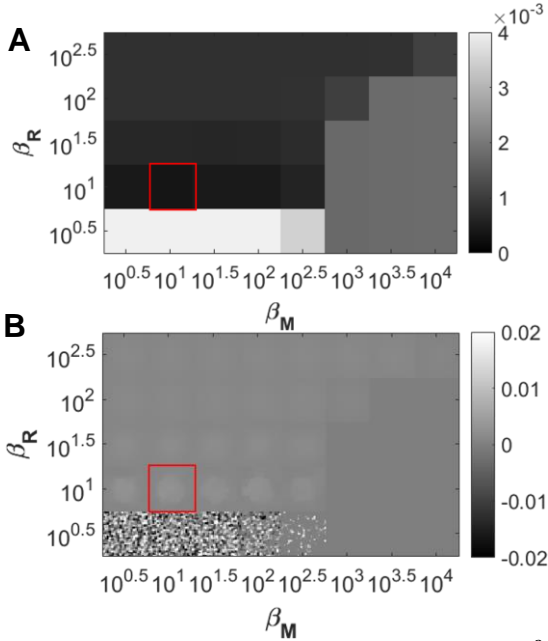
Figure 5: Results of RoD regularization investigation for $I_0 = 10^3$ and $t = 21$ s. (A) Regional RMSE (mm^{-1}) as a function of penalty coefficients β_R and β_M evaluated at a $10^{0.5}$ interval. (B) A zoomed region-of-interest showing difference reconstructions μ_Δ associated with each regularization parameter pair. The red box denotes the optimal β_R and β_M values.

uation of dual liver blood supply components, i.e. hepatic arterial perfusion (HAP) and hepatic portal perfusion (HPP). The HAP was determined as the peak gradient of the hepatic TAC before the peak splenic attenuation (arterial phase) divided by the peak aortic attenuation. (Portal perfusion presumed to be negligible during the arterial phase.) Thus

$$HAP = \frac{F_a}{V} = \frac{\frac{dC_l(t)}{dt}_{max}}{C_a(t)_{max}}, \quad (1)$$

where F_a denotes the arterial flow and $C_a(t)$, and $C_l(t)$ refer to the iodine concentration in artery and liver respectively. HPP was calculated by dividing the peak gradient of the hepatic TAC after the peak splenic attenuation (portal phase) by the peak portal vein attenuation. Mathematically, one can replace F_a and $C_a(t)$ with F_p and $C_p(t)$ in (1) respectively where $C_l(t) = C_a(t) + C_p(t)$. Another common metric, the arterial fraction, or hepatic perfusion index (PI; %), was determined as

$$PI = \frac{HAP + HPP}{HAP}. \quad (2)$$

C. Forward Model

MBIR approaches include RoD require a measurement model. Here, we define mean measurements as

$$\bar{y} = I_0 . exp(-\mathbf{A}\mu), \quad (3)$$

where I_0 is a gain term associated with the unattenuated x-ray fluence for each measurement. The patient anatomy (at a single time point) is denoted by the vector μ, and $\mathbf{A}$ is the system matrix representing the projection operation., We presume an ideal detector so that the random vector y is independent and Poisson distributed.

D. Reconstruction of Difference (RoD)

A brief summary of the RoD method [13] follows. RoD aims to reconstruct the difference image (μ_Δ) between the current
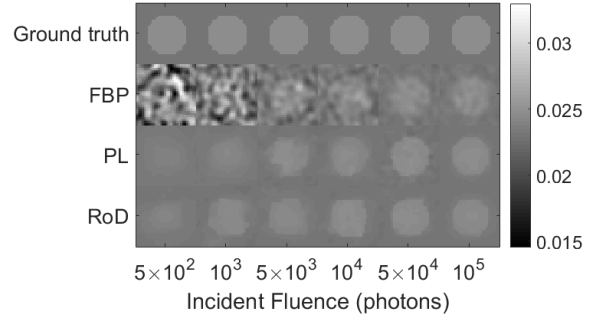
Figure 6: Comparison of different reconstruction methods for incident fluence ranging from 5×10^2 to 10^5 at the $t = 21$ s time point. An ROI of reconstructed volume about the simulated tumor is shown for FBP, PL and RoD.
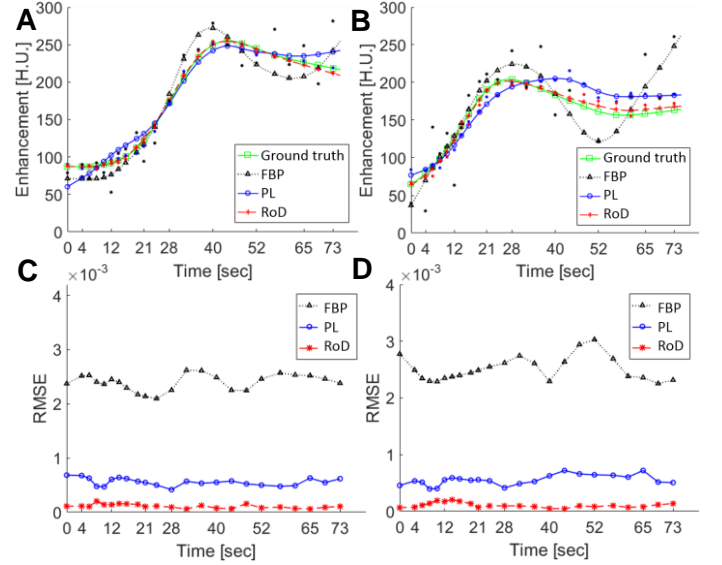
Figure 7: TAC comparison of FBP, PL and RoD reconstructions for the $I_0 = 10^3$ photons case. (A) TAC plot for liver tissue, (B) TAC plot for lesion, (C) RMSE plot for liver TAC and (D) RMSE plot for lesion TAC.

anatomy (μ) and a prior image (μ_p). In CT perfusion imaging, RoD can be employed to reconstruct contrast changes as the difference image between the unenhanced baseline (as a prior image) and individual enhanced images of the same anatomy post-contrast-injection. Under the RoD model

$$\mu = \mu_p + \mu_\Delta. \quad (4)$$

Plugging into the forward model in Eq. (3) yields

$$y = [I_0 \cdot exp(-A\mu_p)] \cdot exp(-A\mu_\Delta) = g \cdot exp(-A\mu_\Delta), \quad (5)$$

where g denotes a new "gain" parameter that includes μ_p. Thus the forward model has a familiar form (same as (3)) and it is straightforward to write a penalized-likelihood objective function for estimation of the difference image, μ_Δ, as

$$\phi(\mu_\Delta; y, \mu_p) = -L(\mu_\Delta; y, \mu_p) + \beta_R \|\Psi\mu_\Delta\|_1 + \beta_M \|\mu_\Delta\|_1, \quad (6)$$

where the log-likelihood function is denoted with L. Two penalty terms are included: 1) an edge-preserving roughness penalty term which encourages the smoothness in the difference image and controlled by a regularization parameter β_R. (Ψ denotes a local pairwise voxel difference operator.) And, 2) a magnitude penalty on μ_Δ which encourages sparseness of the difference image controlled by parameter β_M. The latter penalty also controls the amount of prior information integrated from the unenhanced baseline image since increased sparsity of the change image implies increased similarity to the prior image.

We solve the optimization problem for μ_Δ using separable paraboloidal surrogates (SPS) algorithm with 100 iterations and 10 subsets. All reconstruction methods and evaluation routines were implemented in Matlab (The Mathworks, Natick, MA) with projectors/back-projectors in C/C++ using CUDA libraries for acceleration.

III. EXPERIMENTS

To investigate the performance of the RoD approach in CTP, simulation studies were performed to evaluate different CTP reconstruction methods. Specifically, filtered-backprojection (FBP), penalized-likelihood (PL) [15] reconstruction (100 SPS iterations with 10 subsets, Huber penalty on pairwise differences over a first-order neighborhood, and Huber parameter $\delta = 10^{-4}$ mm^{-1}), and RoD techniques are compared.

A. Regularization Investigation

The RoD objective function includes two coefficients, β_R and β_M, which control the strength of the roughness and prior magnitude penalty, respectively. To study the optimal penalty strength, we performed an exhaustive 2D sweep of these parameters. Optimal parameters based on the RMSE around a region-of-interest (ROI, shown in Figure 3) including the simulated tumor were selected for each time point in the temporal sequence. The same kind of exhaustive search using RMSE was used to optimize the single regularization parameter for PL.

B. Incident Fluence Investigation

To study the performance of RoD under different exposure conditions, we simulated different levels of Poisson noise for noisy measurements with fluence ranging from $I_0 = 5 \times 10^3$ to 10^5 (photons per pixel) in each of the time points. The prior image for RoD was produced by PL reconstruction of the $t = 0$ (unenhanced image volume) using $I_0 = 5 \times 10^3$ photons.

IV. RESULTS

A summary of investigations on the effectiveness of the RoD approach in Liver CT perfusion is presented in the following subsections. Detailed results are presented for the case of $I_0 = 10^3$ photons. This photon level is two orders of magnitude lower than the baseline acquisition.

A. Regularization Investigation

Optimal penalty coefficients for β_R and β_M were computed for all images and exposure levels. The results of a sample 2D parameter sweep for the $I_0 = 10^3$ and $t = 21$ s scenario are shown in Figure 5. Specifically, both the RMSE and the reconstructed region-of-interest difference images are shown as a function of both regularization parameters. One sees increased noise for lower β_R values and increased blur for large β_R values. Similarly, large values of β_M decreases noise; however, values larger than 10^3 prevented the change from appearing in the reconstructed image. The best image quality in terms of RMSE has been achieved by setting $\beta_R = 10$ and $\beta_M = 10$ for this case. Similar patterns emerged for other exposure levels and time points with some variation in optimal parameter values.

B. Incident Fluence Investigation

Figure 6 compares reconstructed ROI images using FBP, PL
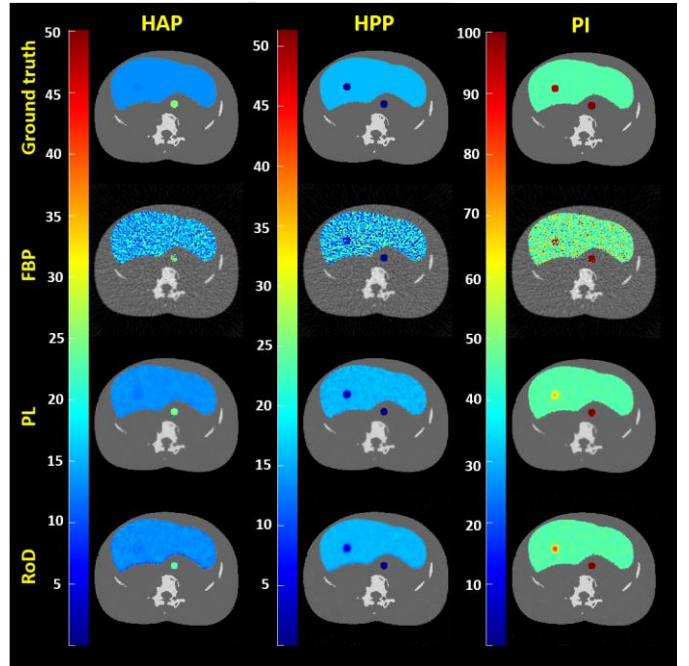
Figure 8: HAP, HPP and PI maps for FBP, PL and RoD reconstruction methods compared to ground truth for an incident fluence of $I_0 = 10^3$ photons.

and RoD reconstruction techniques near the peak of the lesion enhancement curve ($t = 21$ s) for different incident fluence values. The performance of all three methods deteriorated for very low exposures; however, RoD performed consistently qualitatively better than the other methods.

C. Time Attenuation Curves and Reconstructed Images

Focusing on the $I_0 = 10^3$ scenario, we used all time points in the image sequence to form TACs for each reconstruction approach. Smoothed TACs based on a healthy liver and tumor ROIs are shown in Figure 7 for each reconstruction method and ground truth. Stochastic fluctuations observed in the individual time points as well as the TACs are reduced in going from FBP to PL. RoD produces TACs closest to the ground truth with a more substantial improvement for the tumor ROI.

D. Perfusion Maps

Figure 8 shows the perfusion maps including HAP, HPP and PI metrics for each reconstruction method for the $I_0 = 10^3$ scenario. Again, increased noise is evident in the FBP data. This is reduced using PL and further reduced in RoD (particularly for the HPP map). We also note in the PI maps, that there is a loss of contrast at the tumor for PL relative RoD. Overall, perfusion parameters were most accurate for the RoD approach.

V. DISCUSSION

In this paper, we have introduced RoD for low-dose CT perfusion imaging of the liver. The proposed approach estimates the difference between unenhanced baseline and subsequent scans. This use of the baseline as a prior image permits significant reductions in noise in reconstructions. Several experiments evaluating the performance of RoD relative to traditional analytic and MBIR methods suggest that RoD produces better images, better quantitation in the TACs, and better perfusion maps for commonly used perfusion metrics.

These results suggest the RoD processing can dramatically reduce exposure requirements. In this case, the exposure of all but the unenhanced baseline scan was dropped by two orders of magnitude and accurate perfusion results were maintained. Future studies will expand upon these initial studies to determine the limits of dose reduction possible in practical CT systems.

REFERENCES

[1] K. A. Miles, T. Y. Lee, V. Goh, E. Klotz, C. Cuenod, S. Bisdas, A. M. Groves, M. P. Hayball, R. Alonzi, and T. Brunner, "Current status and guidelines for the assessment of tumour vascular support with dynamic contrast-enhanced computed tomography," *Eur. Radiol.*, vol. 22, no. 7, pp. 1430–1441, 2012.

[2] S. H. Kim, A. Kamaya, and J. K. Willmann, "CT Perfusion of the Liver: Principles and Applications in Oncology.," *Radiology*, vol. 272, no. 2, pp. 322–44, 2014.

[3] D. V. Sahani, N.-S. Holalkere, P. R. Mueller, and A. X. Zhu, "Advanced Hepatocellular Carcinoma: CT Perfusion of Liver and Tumor Tissue— Initial Experience [1]," *Radiology*, vol. 243, no. 3, pp. 736–743, Jun. 2007.

[4] E. Liapi, M. Mahesh, and D. V. Sahani, "Is CT perfusion ready for liver cancer treatment evaluation?," *J. Am. Coll. Radiol.*, vol. 12, no. 1, pp. 111–113, 2015.

[5] P. V Pandharipande, G. A. Krinsky, H. Rusinek, and V. S. Lee, "Perfusion Imaging of the Liver: Current Challenges and Future Goals," *Radiology*, vol. 234, no. 3, pp. 661–673, 2005.

[6] M. Okada, T. Kim, and T. Murakami, "Hepatocellular nodules in liver cirrhosis: State of the art CT evaluation (perfusion CT/volume helical shuttle scan/dual-energy CT, etc.)," *Abdom. Imaging*, vol. 36, no. 3, pp. 273–281, 2011.

[7] A. K. Hara, R. G. Paden, A. C. Silva, J. L. Kujak, H. J. Lawder, and W. Pavlicek, "Iterative reconstruction technique for reducing body radiation dose at CT: feasibility study.," *AJR. Am. J. Roentgenol.*, vol. 193, no. 3, pp. 764–71, Sep. 2009.

[8] N. Negi, T. Yoshikawa, Y. Ohno, Y. Somiya, T. Sekitani, N. Sugihara, H. Koyama, T. Kanda, N. Kanata, T. Murakami, H. Kawamitsu, and K. Sugimura, "Hepatic CT perfusion measurements: a feasibility study for radiation dose reduction using new image reconstruction method.," *Eur. J. Radiol.*, vol. 81, no. 11, pp. 3048–54, Nov. 2012.

[9] G.-H. Chen, J. Tang, and S. Leng, "Prior image constrained compressed sensing (PICCS): a method to accurately reconstruct dynamic CT images from highly undersampled projection data sets.," *Med. Phys.*, vol. 35, no. 2, pp. 660–3, Mar. 2008.

[10] J. W. Stayman, H. Dang, Y. Ding, and J. H. Siewerdsen, "PIRPLE: a penalized-likelihood framework for incorporation of prior images in CT reconstruction.," *Phys. Med. Biol.*, vol. 58, no. 21, pp. 7563–82, Nov. 2013.

[11] B. E. Nett, R. Brauweiler, W. Kalender, H. Rowley, and G.-H. Chen, "Perfusion measurements by micro-CT using prior image constrained compressed sensing (PICCS): initial phantom results," *Phys. Med. Biol.*, vol. 55, no. 8, pp. 2333–2350, Apr. 2010.

[12] H. Dang, A. S. Wang, M. S. Sussman, J. H. Siewerdsen, and J. W. Stayman, "dPIRPLE: a joint estimation framework for deformable registration and penalized-likelihood CT image reconstruction using prior images.," *Phys. Med. Biol.*, vol. 59, no. 17, pp. 4799–826, Sep. 2014.

[13] A. Pourmorteza, H. Dang, J. H. Siewerdsen, and J. W. Stayman, "Reconstruction of difference in sequential CT studies using penalized likelihood estimation.," *Phys. Med. Biol.*, vol. 61, no. 5, pp. 1986–2002, Mar. 2016.

[14] K. A. Miles, M. P. Hayball, and A. K. Dixon, "Functional images of hepatic perfusion obtained with dynamic CT.," *Radiology*, vol. 188, no. 2, pp. 405–411, Aug. 1993.

[15] J. A. Fessler, "Statistical image reconstruction methods for transmission tomography," *Med. Image Process. Anal.*, vol. 3, pp. 1–70, 2000.